Draft version July 30, 2018
Typeset using LaTeX **twocolumn** style in AASTeX62

Small scale features in the HD163296 planet forming disk revealed by ALMA

Andrea Isella[1] and et al.[2]

[1] *Rice Univeristy*
[2]

(Revised July 30, 2018)

ABSTRACT

In this paper, we present new ALMA observations of both the dust and 12CO emission of the circumstellar disk around the Herbig Ae star HD 163296. At a distance of 101 pc (Gaia), HD 163296 is in several respects the poster child of disks thought to be perturbed by planets. The star is surrounded by a huge (more than 1000 au in diameter) Keplerian disk whose mass has been estimated to range between XX and YY M⊙ (ref). ALMA observations that resolved the gas and dust emission on spatial scales of 20 au, revealed the presence of three deep circular gaps in the dust emission with radii of 60 au, 100au, and 160 au (Isella et al. 2016). Comparison with planet-disk interaction models suggest that these rings might be carved by three Saturn mass planets orbiting at XX, YY, and ZZ au, respectively (Liu et al. 2018). This hypothesis is supported by the detection of deviation from keplerian rotation in agreement with the presence of pressure maxima created by such planets (Teague et al. 2018). The presence of an additional planet orbiting at ZZ au has been proposed based on deviations in the gas keplerian velocity (Pinte et al. 2018).

1. INTRODUCTION

In recent years, millimeter-wave interferometers and near infrared high contrast cameras have delivered first direct images of planetary systems in the act of forming (ref). Although largely incomplete, these observations inform about the birth radius of planets and the processes responsible for their formation.

The majority of circumstellar disks observed at a spatial resolution better than 50 au reveal ring-like features in the emission of small and large dust particles, as well as of the molecular gas. The homogeneous survey performed as part of DSHARP has revealed that multiple systems of dusty rings are ubiquitous among the most massive circumstellar disks (Andrews et al.). Both the number of rings and their structure varies substantially from object to object, and in some cases, even within the same disk (Huang et al.).

A myriad of theoretical models have been proposed to explain the formation of rings in circumstellar disks. These include the interaction between the disk and yet-unseen planets (ref), sharp opacity variations at gas-solid phase transitions (ref), dust accumulations at the edge of magneto-rotational instability dead zones, and hydrodynamic instabilities (ref). However, to date, the planet-disk interaction model has been the most successfull in reproducing most of the observed (ref). Furthermore, young planet candidates in ringed disks have been directly detected at infrared and optical wavelenghts (PDS70, LkCa15, etc.).

These results pose two theoretical problems. Firstly, since ringes are observed in disks as young as 1 Myr, they would imply giant planets to form on timescales shorter than predicted. Secondly, since rings radii as large as about 200 au have been measured, they would imply the presence of a large population of wide separation planets. This seems to be in conflict with the very low fraction (1%) of wide separation giant planets observed around main sequence stars (Bowler et al. 201?).

Corresponding author: Andrea Isella
isella@rice.edu

2. OBSERVATIONS

Data acquisition and calibration

Data selfcalibration and imaging

3. RESULTS

3.1. *Dust continuum*

Figure 1 shows the map of the 1.3 mm dust continuum emission imaged with a synthesized beam FWHM of $0.045'' \times 0.055''$, corresponding to a spatial resolution of 4.5×5.5 au at the distance of the source. The image features two bright elliptical rings previously reported by Isella et al. (2016), as well as three new morphological features: an arc of emission inside the first bring ring (inset a), an inner continuum ring with a radius of about 15 au, and a central azimuthal asymmetry (inset b). In this section we firstly discuss the morphology of the continuum rings and then constrain the amount of azimuthal asymmetries visible in the image.

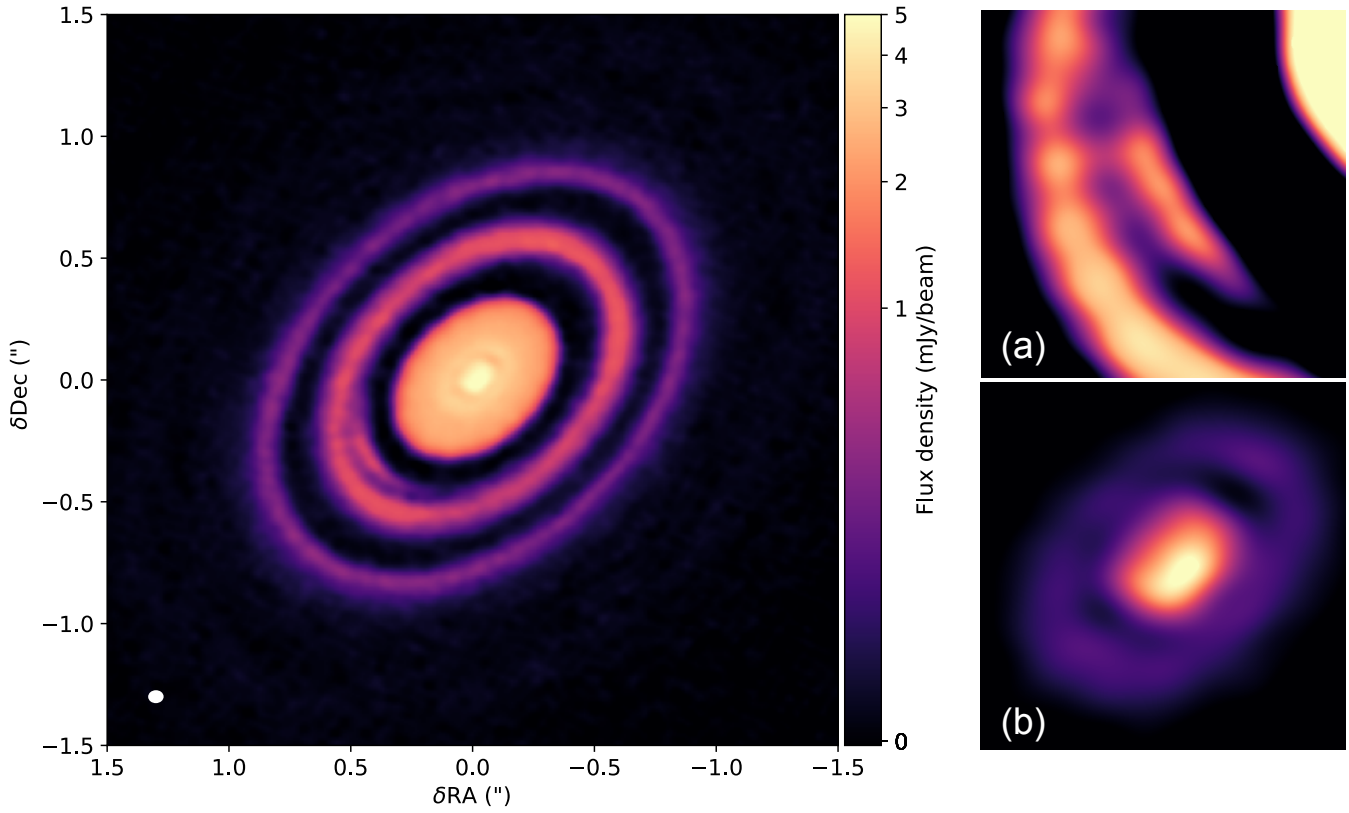

Figure 1. Map of the HD 163296 disk recorded in the 1.3 mm continuum. The angular resolution of the observations is $0.045'' \times 0.055''$and is indicated by the white ellipse in the bottom right corner. Inset (a) and (b) show zoom-in view of two asymmetric features revealed by the observations. The rms noise is 0.0165 mJy/beam

Morphology of the dust rings: We fit bright and dark rings with ellipses defined by the position of the center (Δx_0, Δy_0), the semi-major axis r, the aspect ratio s or, equivalently, the inclination i of the line of sight at which a circular ring will appear as an ellipse with aspect ratio s ($s = \cos i$), and a position angle (PA) increasing from East of North. The fit is performed following the procedure discussed in Huang et al. (2019). In brief, we locate the points (x,y) corresponding to the crest or through of each ring, and use the python *emcee* package to calculate the ellipses that best reproduce this set of points. The best fit parameters are listed in Table 1 and are the same of those reported by Huang et al. (2018). Bright and dark rings are indicated with the suffixes BR and DK, respectively, while the number appearing in the ring label corresponds is the ring radius in au. The uncertainties on the best fit values correspond to the 16th and 84th percentile of the marginalized posterior probability distribution.

Overall, the bright and dark rings are well described by ellipses characterized by the same inclination and position angle. A weighted average returns a mean inclination of $(46.4 \pm 0.1)^\circ$ and a position angle of $(133.3 \pm 0.1)^\circ$. Using these value, we deproject the continuum intensity map and obtain the polar map shown in Figure 2) where $\theta = 0$ indicates the direction of the apparent disk minor axis. Here, the bright rings BR68, BR100, and BR160, appear as vertical stripes of constant radius.

The elliptical fitting indicates that DK45 and DK10 have significantly lower inclinations of 42.3° and 28.5° respectively. In the case of DK45, the fitting is likely affected by the emission arc that extends in azimuth from $-125^\circ < \theta < -75^\circ$. The characteristics of this feature are discussed below. The lower inclination of DR10 might instead result from the fact that this dark ring vanishes along the disk minor axis ($\theta = 0, \pm 180$) where, due to the finite angular resolution of the observations, it is filled by emission coming from the surrounding disk regions.

Table 1. Properties of dark and bright rings

Feature	Δx_0 ($''$)	Δy_0($''$)	r(")	r(au)	i(°)	PA(°)
(1)	(2)	(3)	(4)	(5)	(6)	(7)
BR160	-12±11	9.0±10.0	1.582±0.013	159.8±1.0	47.1±0.8	132.6±1.2
BR100	-2.3±0.6	9.0±0.6	0.9867±0.0007	99.66±0.07	46.4±0.1	133.4±0.1
BR68	-5.6±0.7	7.3±0.7	0.6642±0.0009	67.08±0.08	46.6±0.1	133.1±0.2
BR15	-7.8±0.9	9.8±0.7	0.1439±0.0008	14.53±0.07	46.3±0.8	131.7±0.9
mean BR	-4.5±0.4	8.8±0.4	-	-	46.4±0.1	133.3±0.1
DK143	-6.3±7.3	26.9±6.9	1.418±0.009	143.25±0.69	48.1±0.6	133.4±0.8
DK87	-0.9±1.6	4.4±1.6	0.8592±0.0021	86.77±0.16	47.2±0.2	133.1±0.3
DK45	-4.5±1.4	3.7±1.3	0.4450±0.0017	44.95±0.13	42.3±0.4	132.5±0.6
DK10	-10.6±1.0	8.2±0.8	0.1029±0.0009	10.49±0.08	28.5±1.4	102.9±5.3
mean DK*	-3.1±1.0	4.4±1.0	-	-	46.1±0.2	133.0±0.3
mean*	-4.3±0.4	8.2±0.4	-	-	46.4±0.1	133.3±0.1

NOTE—*DR10 parameters are not used to calculate average values

Table 2. Intensity ratios

Pair	Maj	Min	Mean
(1)	(2)	(3)	(4)
BR15/DK10	1.15	0.96	1.03
BR68/DK45	38.71	7.49	16.81
BR100/DK87	10.68	4.51	6.48
BR160/DK143	1.47	0.90	1.37

NOTE—(1) Pair of rings. (2) Intensity ratio along the apparent disk major axis. (3) Intensity ratio along the apparent disk minor axis. (4) Intensity ratio of the azimuthally averaged intensity profile

The effect of beam smearing is clearly visible by comparing the radial profile of the continuum emission measured along the disk major and minor axes (Figure 3). In the case of the innermost pair of rings, the intensity ratio is $I(BR15)/I(DK15) = 1.15$ along the major axis and 0.96 along the minor axis. The intensity ratios for all the pairs of rings are listed in Table 2

Model fitting in the uvplane: ongoing

Azimuthal asymmetries: In the bottom panel of Figure 2 we highlight the azimuthal asymmetries in the dust emission by plotting the difference between the deprojected intensity and its azimuthal average. The brightest feature is an excess of emission centered at $r \sim 55$au, and extending between about 80°and 120°in azimuth (see also panel b of Figure 1). A second bright asymmetry is observed in the innermost disk region.

3.2. *12CO J=2-1*

Figure 5 shows channels maps of the ^{12}CO (2-1) emission mapped at an angular resolution of $0.95'' \times 0.10''$ and velocity resolution of 0.32 km s^{-1}. The rms noise is 0.85 mJy/beam per channel.

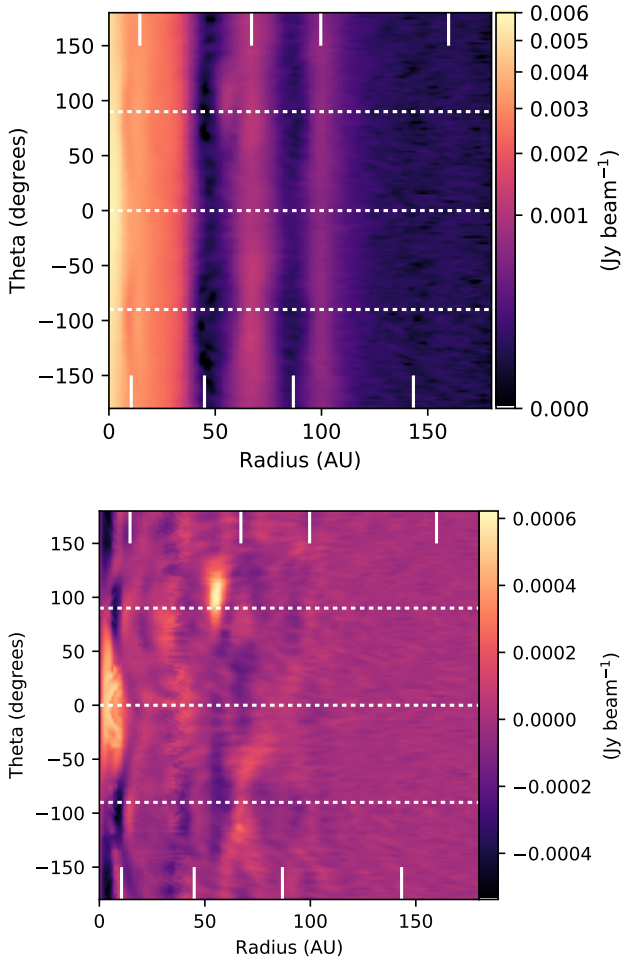

Figure 2. Polar map of the 1.3 mm dust continuum emission deprojected for the disk inclination using an inclination value of 46.4°

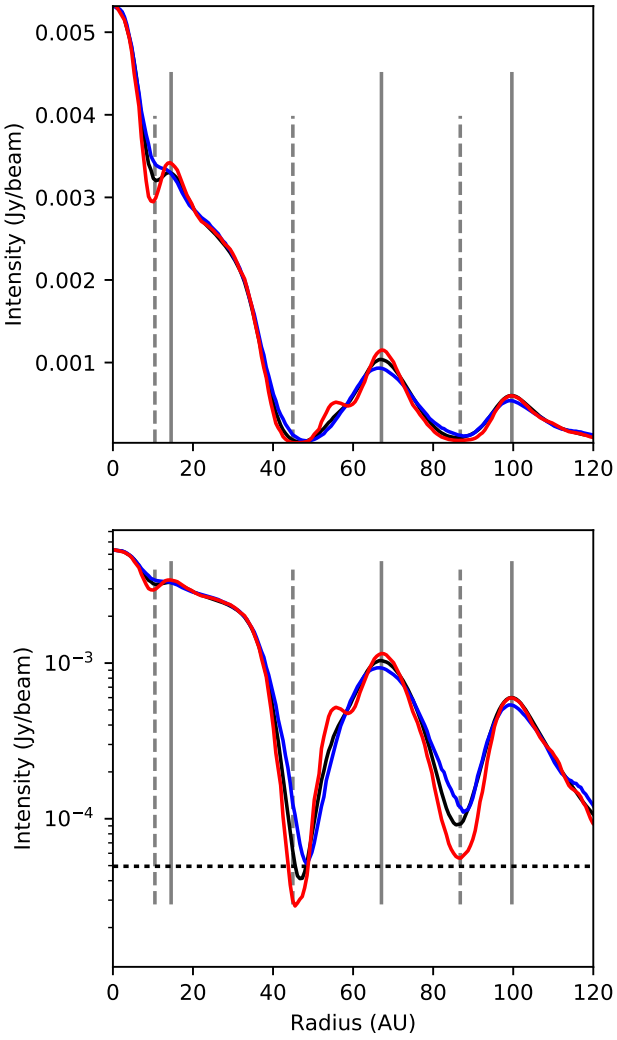

Figure 3. Deprojected radial profile of the 1.3 mm continuum emission. The black lines show the azimuthal average, while the red and blue lines show the radial profile along the disk major and minor axis, respectively. The top and bottom panel show the intensity on linear and logarithmic scales respectively. Vertical dotted lines indicate the position of the dark rings, while vertical solid lines indicate the position of bright rings. Finally, the horizontal dotted line indicates the intensity level corresponding to 3× the rms noise.

Figure **??** shows the integrated spectrum, the integrated intensity (zeroth moment of the emission) and the velocity centroid (first moment of the emission). The rms noise of the 12CO maps is 0.85 mJy/beam per channel.

4. DISCUSSION

- Calculate and discuss optical depth of the bright rings by comparing the brightness temperature with temperature model by Isella et al. (2016), Rosenfeld et al. (2014), Flaherty et al. (2016) (see also Liu et al. (2018). Calculate optical depth of the bright rings from the absorption of CO coming from the disk back side.

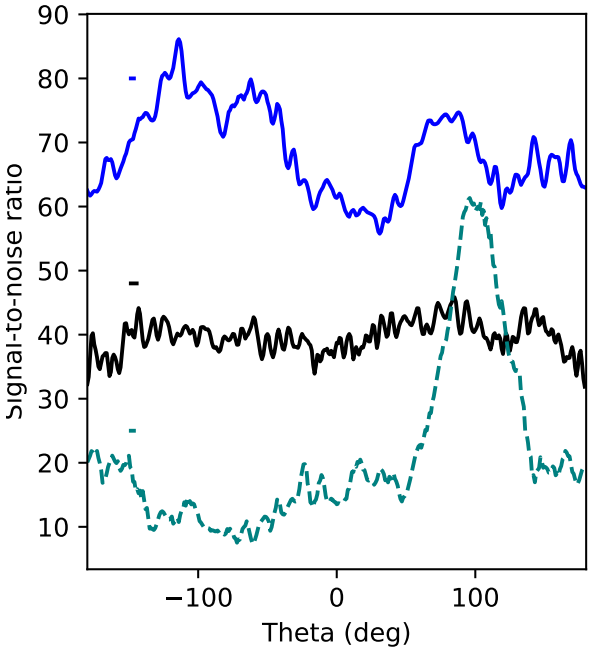

Figure 4.

- Discuss the new results in the context of planet-disk interaction models (Isella et al. 2016, Liu et al. 2018, Teague et al. 2018, Pinte et al. 2018.) Do we confirm Pinte et al. kink in the CO emission? Do we detect deviations from Keplerian rotation? Connect to Zhauhuan's simulations of planet disk-interaction.

- Discuss upper limits for the detection of circumplanetary disks (e.g. at the position of the putative planet proposed by Pinte et al.)

5. CONCLUSION

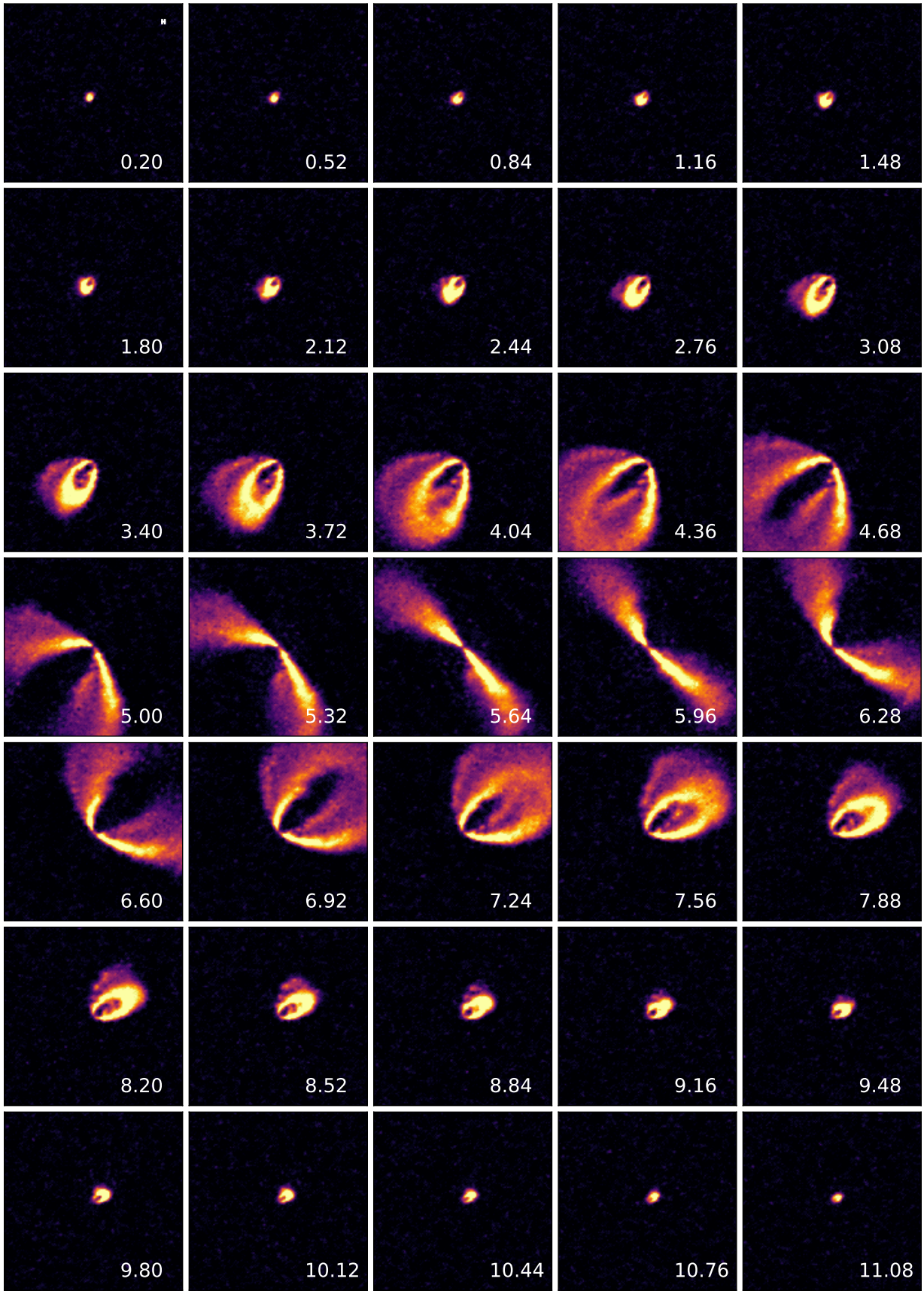

Figure 5. Map of the emission recorded in the 12CO line. The beam FWHM is $0.104'' \times 0.095''$. Color scale is linear.

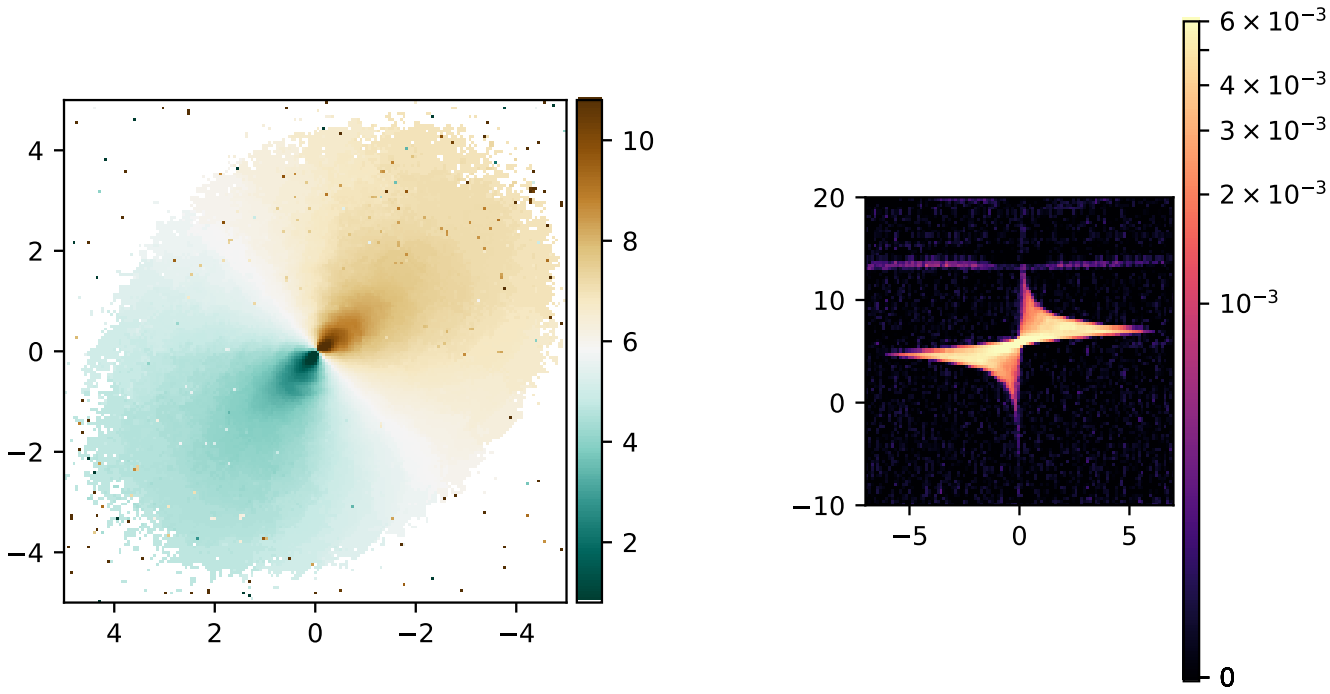

Figure 6. Moment 1 and pv diagram

REFERENCES

Isella, A., Guidi, G., Testi, L., et al. 2016, PhRvL, 117, 251101